Electron localization and charge transport in poly(*o*-toluidine): A model polyaniline derivative

Zhao H. Wang
Department of Physics, The Ohio State University, Columbus, Ohio 43210-1106

Anjan Ray* and Alan G. MacDiarmid
Department of Chemistry, University of Pennsylvania, Philadelphia, Pennsylvania 19104

Arthur J. Epstein
Department of Physics and Department of Chemistry, The Ohio State University, Columbus, Ohio 43210-1106
(Received 20 July 1990)

The electron localization is increased with increasing one dimensionality of a quasi-one-dimensional disordered system (quasi-1D-DS). This concept is tested by studying the electron localization in the methyl ring-substituted derivative of polyaniline (PAN), poly(*o*-toluidine) (POT). The studies include the measurements of temperature dependence of the dc conductivity $\sigma_{dc}(T)$, thermoelectric power $S(T)$, microwave conductivity $\sigma_{mw}(T)$, and dielectric constant $\epsilon(T)$ at 6.5 GHz, dc susceptibility $\chi(T)$, electron paramagnetic resonance, and electric-field dependence of conductivity $\sigma(F)$. The experimental results showed greater electron localization in the HCl salt of POT than that of PAN, reflected in much smaller σ_{dc}, σ_{mw}, and ϵ, increased Curie susceptibility, and decreased Pauli-like susceptibility. The localization is attributed to the reduced interchain diffusion rate caused by decreased interchain coherence and increased interchain separation, both of which result from the presence of CH_3 on the C_6 rings. The T dependences of $\ln\sigma \sim -T^{-1/2}$ and $S(T) \sim S_0 + B/T$ are interpreted as quasi-1D variable-range hopping (VRH) between the nearest-neighboring chains. Within the model, $\sigma(F) \sim \mathcal{H}F^{1/2}$ with $\mathcal{H} \sim T^{-1/2}$ can be understood. The charging energy limited tunneling model for granular metals and the three-dimensional VRH model with a Coulomb gap are not consistent with the experiments. Other possible mechanisms for electron localization and the general implications for control of dimensionality and conductivity are discussed.

I. INTRODUCTION

Isolated chains of conducting polymers are one-dimensional (1D) entities. Models based on this 1D character have accounted for many of their unusual spectroscopic and magnetic phenomena, attributed to the presence of solitons and polarons.[1,2] It is well known, however, that due to the interference of scattered electron waves, all the electron states in a strict one-dimensional disordered system (1D-DS) are localized with any weak disorder.[3–6] The localized electron wave function in a strictly 1D-DS decays exponentially from its center. This was pointed out by Mott and others[3,4] and proved later by rigorous calculations.[5] For localized states dc conductivity $\sigma_{dc}=0$ at the $T=0$ K limit, while for metals σ_{dc} is finite. The strictly 1D model fails to represent polymers (for instance, polyacetylene) which show "metallic" behavior upon doping.[7–9] The reason for the metallic behavior is that these polymer systems are not strictly 1D, but quasi-1D systems where interchain coupling is not negligible. In this paper we will explore the importance of the interchain coupling on electron localization in a quasi-1D-DS, poly(*o*-toluidine). Our results demonstrate the essential role of coherent interchain coupling in control of localization in a quasi-1D-DS.

The strength of the interchain coupling is characterized by interchain diffusion rate or interchain transition rate w. If an electron can coherently transfer from one chain to another before it is reflected back by an impurity or chain defect the electron may avoid the interference of backward scattering of electron wave functions and hence decrease the localization. It can be shown[6,7,10] that in the case of weak disorder, i.e., $E_F\tau_i/\hbar \gg 1$ where E_F is the Fermi energy, τ_i is the mean free time, and $\hbar$ is Planck's constant divided by 2π, if the interchain diffusion rate w exceed a threshold value w_c, the states become extended; otherwise they are still localized.[6] In the localized regime, i.e., $w < w_c$, the interchain coupling increases the localization length α^{-1} of electron states.[6,11] In the case $w \sim w_c$, α^{-1} is increased by a factor of $w/(w_c - w) \gg 1$. If the disorder is not "weak," $E_F\tau_i/\hbar \sim 1$, the interchain diffusion still tends to delocalize the electron wave function though an insulator-metal transition may not occur.[12]

The value of the diffusion rate w depends on many parameters. In the weak interchain coupling case $w \ll w_c$, $w \sim 2\pi t_\perp^2 \tau_i/\hbar^2$ if the chains are packed into a perfect lattice[7,13] ($t_\perp$ is the interchain tansfer integral or $\frac{1}{4}$ of the interchain bandwidth). Hence in the case of a perfect chain packing, w depends on $t_\perp$ and τ_i. It can be shown[6,13] that when $t_\perp$ or τ_i increases so that $t_\perp\tau_i/\hbar = 0.3$, w will be equal to w_c and an insulator-metal transition occurs. It is

noted that $t_\perp$ is related to the overlap of the electron wave functions at two neighboring chains. This overlap is an exponentially decaying function of interchain distance. Hence the interchain separation is expected to be of considerable importance in the localization of a quasi-1D-DS. The value of τ_i depends on the concentration of defects and intrachain crystalline coherence length. The importance of τ_i in determination of conductivity of a conducting polymer has been realized by many authors (see Refs. 6–9, 11, 13, and 14). Highly stretched I_2-doped "new" polyacetylene has very high conductivity which is likely attributed to the reduction of defects and improvement in crystalline coherence length.[7,8] In the case where interchain disorder is present, interchain crystalline coherence length is another important parameter in electron localization of a quasi-1D-DS. The coherent transfer of an electron from one chain to another will be interrupted by the interchain disorder and the electrons will be localized transversely to some extent and a smaller w is expected.[7]

The polyaniline (PAN) system provides an excellent quasi-1D-DS system to test the above concepts. With substitution of a methyl group (CH_3) for a hydrogen atom on each C_6 ring of the emeraldine salt form of PAN (PAN-ES), the poly(*o*-toluidine) salt (POT-ES) is formed[15] (Fig. 1). The optical spectra[15] change only slightly, reflecting a small increase in ring angle due to increased steric repulsion from the CH_3 groups.[2] Also crystallinity and *intrachain* coherence length are similar.[16,17] However, within the crystalline regions of POT-ES there is greater disorder in the *interchain* separation[16] compared with that of PAN-ES, likely associated with the random location of CH_3 at the (a) and (b) atom of the C_6 (see Fig. 1) and there is a few percent increase in interchain separations.[16] So the *interchain* transfer integral $t_\perp$ of POT-ES and *interchain* coherence are decreased, but the *intrachain* band structures and *intrachain* coherence length remain essentially the same.[15–17] Both interchain effects tend to decrease the interchain diffusion rate and hence increase localization of the electron states. Therefore it is expected that the electron states in POT-ES will be more localized than those in PAN-ES.

In this paper we report systematic studies of electron localization in the POT-ES system by magnetic susceptibility $\chi(T)$, dc conductivity σ_{dc} (both temperature and electric-field dependence), microwave conductivity $\sigma_{MW}(T)$ and dielectric constant $\epsilon(T)$, thermopower $S(T)$ and electron-spin-resonance measurements. It completes our results briefly reported earlier.[18] Although there is no significant difference of the electron band structures of PAN-ES and POT-ES, our transport and magnetic studies confirmed the increased localization of charges in POT-ES associated with reduced interchain diffusion rate. Quantitative data analyses show that quasi-one-dimensional variable-range hopping (quasi-1D VRH) of the charge carriers between the nearest-neighboring chains is responsible for charge transport. The estimated localization length is several Å. The data do not support either the charging limited tunneling model[19] or 3D VRH with a Coulomb gap.[20]

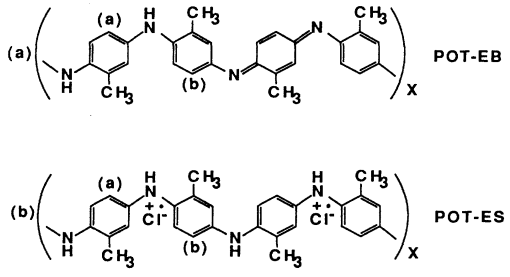

FIG. 1. Schematic structure of (a) POT-EB, (b) POT-ES, doped with 1*M* HCl solution. Note that one H atom on each C_6 ring in PAN is replaced by CH_3 group in POT. Due to ring torsional motion about the N-N axis, there are two possible locations for the CH_3 [(a) and (b)] on each C_6 ring.

This paper is organized as follows. In Sec. II we discuss theoretical models for quasi-1D-DS. We limit our discussion only to the models relevant to our experiments. In Sec. III we present our experimental results. In Sec. IV we will analyze our experimental data based on these theoretical models. In Sec. V localization mechanisms are discussed. Finally in Sec. VI we draw our conclusion.

II. QUASI-ONE-DIMENSIONAL DISORDERED SYSTEMS, MODELS

A. dc conductivity

Let us consider a quasi-1D-DS in which charges are transported effectively along one-dimensional chains. These chains are assumed to have finite length and pack parallel into bundles. If the disorder is weak, i.e., $E_F\tau_i/\hbar \gg 1$, there exists a threshold value of interchain transition rate w_c, below which ($w < w_c$) the electron states are localized and above which ($w > w_c$) they are extended.[6,7] In the localized regime, the conduction at finite temperatures is due to so-called phonon-assistant hopping. Specifically, at low temperatures $k_BT \ll \hbar/\tau_i$, Mott's variable-range hopping among the localized states dominates the conduction.[4,5,13] For a strict 1D-DS, VRH conductivity varies as $\ln\sigma \sim T^{-1}$.[21] But for a quasi-1D-DS near the insulator-metal transition ($w \sim w_c$) where the electron wave functions are extended over several chains, there exists a fairly high temperature, below which the quasi-1D-VRH conductivity along the chains is given by[13,22]

$$\sigma = \sigma_0 \exp[-(T_0/T)^{1/2}] \tag{1}$$

and

$$\sigma_0 = \frac{e^2 \nu_{ph}}{\alpha k_B T A}, \quad T_0 = \frac{8\alpha}{g(E_F)k_B}, \tag{2}$$

where e is the electron charge, ν_{ph} is the attempting frequency, k_B is Boltzmann's constant, $g(E_F)$ is the density of states with one sign of spin (since phonons are spinless so that electron spins are approximately conserved during the hopping processes), and A is the average cross-sectional area of each chain.

Note that ν_{ph} may be a function of temperature, depending on details of electron-phonon interactions.[4,13] Mott and Davis[4] took it as a constant. Nakhmedov, Prigodin, and Samukhin[13] gave $\nu_{ph} \propto T^p$ and $p \geq 1$. The preexponential factor can be calculated, in principle, from the resistor network model proposed by Miller and Abrahams[20,23] for single-phonon hopping processes. This model give an upper limit of ν_{ph} on the order of the phonon frequency,[4] but ν_{ph} decreases rapidly with increasing hopping energies or temperatures.[4,20] Therefore at high temperatures the contribution to the conductivity from single acoustic phonon hopping processes may be smaller than that of multiphonon hopping processes.[4,24] The latter may be important in many noncrystalline materials where hopping energy is in the range of 10^{-2}–10^{0} eV.

For weak interchain coupling, i.e., $w \ll w_c$ or $t_\perp \tau_i \ll \hbar$, it is shown[13] that longitudinal localization length $\alpha^{-1}=4l_i$ and transverse localization length $\beta^{-1}=b$ where l_i is longitudinal mean free path and b is the interchain separation. Since the probability of a charge hopping beyond the nearest-neighboring chains is very small in the case of weak interchain coupling (though there is "variable-range" hopping along the chain direction), we can consider the VRH between the nearest-neighboring chains only. Interchain hopping conductivity perpendicularly to the chains is[13]

$$\sigma_\perp = \frac{2e^2 g(E_F) b^2 \nu_{ph}}{A} (t_\perp \tau_i/\hbar)^2 \exp[-(T_0/T)^{1/2}] , \quad (3)$$

where

$$T_0 = 8\alpha/g(E_F) z k_B , \quad (4)$$

where z is the number of nearest-neighboring chains. The most probable hopping distance (R_{opt}) and hopping energy (W) are

$$R_{opt} = \frac{\alpha^{-1}}{4}(T_0/T)^{1/2}, \quad W = \frac{k_B}{2}(T_0 T)^{1/2} . \quad (5)$$

For the component of interchain hopping conductivity parallel to chain direction, the interchain hopping distance $\sim R_{opt}$ is used instead of b and we obtain

$$\sigma_\parallel = \frac{e^2 \nu_{ph}}{\alpha k_B T z A} (t_\perp \tau_i/\hbar)^2 \exp[-(T_0/T)^{1/2}] . \quad (6)$$

In contrast, intrachain VRH conductivity[13] (without any interchain motion allowed) is the same as that of a strict 1D-DS, i.e.,

$$\sigma_{intra} = \frac{2e^2 g(E_F) \nu_{ph}}{A\alpha^2} (zT_0/16T) \exp(-zT_0/16T) . \quad (7)$$

The hopping energy is obviously $W \sim zk_B T_0/16$.

For weak interchain coupling, $t_\perp \tau_i/\hbar \ll 1$, interchain $\sigma_\perp$ and $\sigma_\parallel$ [Eqs. (3) and (6)] are much smaller than intrachain σ_{intra} [Eq. (7)]. *Due to finite chain lengths and occasional large intrachain barriers, it is expected that the observed temperature dependence of the conductivity for an experiment is determined by interchain hopping.*

B. Thermoelectric power

Thermoelectric power in the case of hopping conduction is not well understood and different authors give different results.[4,25] In general, the thermoelectric power S for hopping conduction is given by[4]

$$S(T) = \frac{k_B}{2e}\frac{W^2}{k_B T}\left[\frac{d\ln f(E) g(E) \mu(E)}{dE}\right]_{E_F} , \quad (8)$$

where W is the range of energy contributing to the conduction, $f(E)$ the energy distribution of conduction electrons, and $\mu(E)$ their mobility. According to Mott and Davis,[4] W is assumed to be the hopping energy. For the interchain hopping in quasi-1D-VRH, $W \sim k_B (T_0 T)^{1/2}$ [see Eq. (5)]

$$S(T)_{inter} \approx \frac{k_B^2}{e} T_0 \left[\frac{d\ln f(E) g(E) \mu(E)}{dE}\right]_{E_F,inter} \sim \text{const} \quad (9)$$

and for the intrachain hopping, $W \sim k_B T_0$

$$S(T)_{intra} \approx \frac{k_B^2}{e}\frac{T_0^2}{T}\left[\frac{d\ln f(E) g(E) \mu(E)}{dE}\right]_{E_F,intra} \sim 1/T . \quad (10)$$

The total thermopower will have contributions from both interchain and intrachain hopping and have the T dependence

$$S(T) = S_0 + B/T . \quad (11)$$

For metallic conduction, $W \sim k_B T$. We then have the well-known linear relation $S(T) \propto T$. For 3D-VRH, $W \sim k_B (T_0 T^3)^{1/4}$, $S(T) \propto T^{1/2}$.[4]

C. ac conductivity and dielectric constant

The simplest and most widely used model for ac hopping conductivity is the pair approximation.[26] However, the pair approximation is only valid for high frequencies and it incorrectly predicts $\sigma(\omega) \to 0$ when the frequency $\omega \to 0$. In the low-frequency limit, the conductivity should approach the results obtained by percolation theory which are identical with the results given in Sec. II A within a numerical coefficient.[13,26] It was found that the relation

$$\sigma(\omega) = \sigma_{dc} + \sigma_p(\omega) , \quad (12)$$

where σ_{dc} is calculated by the percolation approach and $\sigma_p(\omega)$ is calculated from pair approximation, gives a good approximation to the conductivity over a wide range of ω.[26]

Following the approach of Mott and Davis[4] for 3D hopping, the pair approximation for 1D hopping gives

$$\sigma_p(\omega) = \frac{e^2 N(E_F)^2}{96\alpha^3 A} k_B T \omega \ln^2(\nu_{ph}/\omega) , \quad (13)$$

where $N(E_F) = 2g(E_F)$ is the density of states with both sign of spins.

At the $T=0$ limit and for $\omega\tau_i \ll 1$ the dielectric constant of a 1D-DS is[5]

$$\epsilon \approx \epsilon_\infty + (2.4) 16 e^2 l_i^2/\hbar v_F A \quad (14)$$

and the localization length $\alpha^{-1}=4l_i$,[5] where ϵ_∞ is the contribution from core polarization. The numerical coefficient depends on details of the calculation and somewhat differing numbers were obtained by other authors.[27] Since $N(E_F)=2/\pi\hbar v_F$ in 1D we can write, including a geometric factor f accounting for the orientation of 1D chains,

$$\epsilon\approx\epsilon_\infty+1.2\pi f e^2 N(E_F)\alpha^{-2}/A \ , \tag{15}$$

where $f\sim\frac{1}{3}$ for random oriented permanent dipole moments. If disorder is not "weak," the relation $\epsilon\propto l_i^2$ still holds, but the numerical coefficient may be slightly different.[5]

The above results can be generalized. If ζ is the localization length in the direction of the electric field (if the external field is perpendicular to the polymer chains, ζ will be the localization length transverse to the chains), a rough estimate of the dielectric constant will be[28]

$$\epsilon\approx\epsilon_\infty+e^2N(E_F)\zeta^2 \ . \tag{16}$$

In the case of transverse polarization $\zeta\sim\alpha_\perp^{-1}$.

III. EXPERIMENTAL TECHNIQUES

POT was synthesized in the base form (POT-EB) (see Fig. 1) as described earlier.[15] The measured POT-ES samples were protonated to approximate 50% ([Cl]/[N]=0.5) by equilibrating the powder samples with 1M HCl solution for a minimum of two days and subsequently drying overnight in vacuum ($\sim10^{-5}$–10^{-4} mbar). Pressed pellets (pressed under a pressure of ~9 kbar) were used for most of the transport measurements, with the exception of microwave studies where films cast from N-methyl-2-pyrrolidinone (NMP) were used. All the samples were handled in the air except the ones used for electron-paramagnetic-resonance (EPR) measurements.

A four-probe technique was utilized for σ_{dc} measurements. The four probes are gold wires attached to the sample surfaces by Acheson Electrodag 502. The electric current was provided by a Keithley 220 current source and a Keithley 194A multimeter was used to measure the voltage. The input resistance of the multimeter is greater than 1 GΩ. The temperature was controlled by a LakeShore DRC 82C temperature controller. Both temperature-sensing diode and sample are contained in a cylinder made of oxygen-free high-conductivity copper. The whole system was enclosed in a Janis DT dewar with He exchange gas. The same system was used for electric-field dependence of conductivity measurements. A HP 214B pulse generator was used to apply a pulsed voltage to the samples and a HP 7603 oscilloscope was used for the measurement. Maximum average input power to the sample from the pulse generator was 10 μW. To reduce sample heating effects due to the applied voltage, samples were in thermal contact with a block of single-crystal quartz through GE 7031 varnish. The displayed temperature fluctuation was on the order of 0.1 K, but due to the large size of the quartz block attached to the samples the actual temperature fluctuation of the samples was expected to be less than that. During the experiment the width and the repetition rate of the pulses from the pulse generator were changed to monitor the heating effects.

A similar probe was used for thermoelectric power measurements. The sample was mounted across two single-crystal quartz blocks maintained at two different temperatures. The temperature difference was no larger than 1 K and was maintained by a Keithley 220 current source. A copper-Constantan thermocouple was also mounted to monitor the temperature difference. During the measurement the temperature difference was slowly increased to 1 K in 5–10 min. The thermovoltages of the samples and thermocouple were measured by two Keithley 180 nanovoltmeters with input resistance larger than 1 GΩ and recorded by a HP 7004B X-Y recorder. The slope of the thermovoltage of the samples versus that of the thermocouple yields the sample thermopower after correction for contact contribution.[29]

The "cavity perturbation" technique was adopted for the microwave frequency transport measurement.[30] A cylindrical TM_{010} cavity of resonance frequency of 6.5 GHz was used. This system has been used to study PAN as well.[31] The microwave source was a HP 8350B sweep generator. A temperature-sensing diode was attached to the outside wall of the cavity to measure the temperature. Since the system was filled with He gas, we assume the temperature of the diode and the sample is the same. The samples were held in quartz tubes. The typical sample size is about $0.5\times0.5\times4$ mm^3. For all the samples the "depolarization regime" condition was satisfied.[30,31]

EPR X-band measurements utilized a Bruker EPS 300 spectrometer with an Oxford ESR900 cryostat.[32] A TE_{104} double rectangular cavity was used. The sample g factor was calibrated by a diphenylpicrylhydrazyl (DPPH) sample. The temperature was controlled by an Oxford ITC4 temperature controller. The static susceptibility was measured by the Faraday technique and the same system has been used to measure the susceptibility of PAN.[33] The core diamagnetic susceptibility was calculated based on the measured value of PAN-EB,[33] with correction for substituents and counterions obtained from Pascal constants.[34]

IV. EXPERIMENTAL RESULTS

We present here the results of comprehensive transport and magnetic studies of the poly(*o*-toluidine) polymer. The absolute static susceptibility of POT-ES after correction for the core diamagnetism is shown in Fig. 2 where the data are plotted as χT versus T. Figure 3 shows the electron-paramagnetic-resonance relative susceptibility of POT-ES and POT-EB obtained by double integration of the EPR signals. After subtraction of the core diamagnetic contributions, the static χ of POT-ES can be decomposed as

$$\chi=\chi_{\text{Pauli}}+C/T \ , \tag{17}$$

where $\chi_{\text{Pauli}}=54\times10^{-6}$ emu/mol (2 ring as a unit) and $C=0.025$ emu K/mol. The χ of POT-EB is roughly Curie-like though more complicated behavior is present

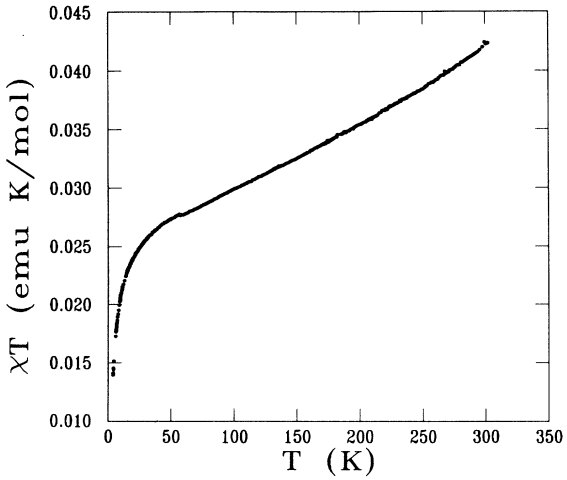

FIG. 2. Temperature dependence of static susceptibility χ of POT-ES per mole (2 ring units) plotted as products of χ and T vs T.

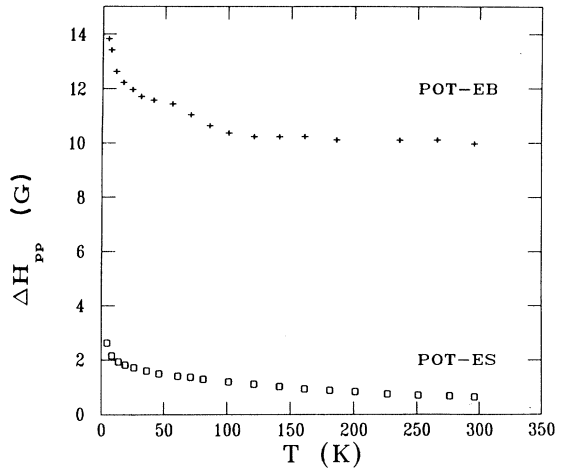

FIG. 4. Temperature dependence of EPR peak-to-peak linewidth of POT-EB (+) and POT-ES (□).

at low temperatures ($T < 100$K), likely due to residual oxygen in the sample. The EPR signal indicates that spin concentration in POT-EB is low (of the same order as for PAN-EB). The data in Fig. 2 show a deviation of χ for POT-ES from Eq. (17) at low temperatures ($T \sim 20$ K).

The EPR linewidths of POT-EB and POT-ES are displayed in Fig. 4. The peak-to-peak linewidth for POT-ES starts with 0.69 at 295 K and increases to 2.4 G monotonically as the temperature is decreased to 4 K, while the linewidth for POT-EB increases from 10 to 14 G over the same temperature range.

The EPR g factor for POT-EB is 2.0050 at 295 K and decreases to 2.0045 at 4 K while the g factor of POT-ES is 2.0034. It only slightly increases when the temperature is decreased (Fig. 5).

The shape of the EPR absorption signal of POT-ES is plotted in Fig. 6, together with that of PAN-ES. The y axis is the reciprocal intensity (single integral of EPR derivative signal) normalized to its central value and the x axis the square of the static magnetic field measured from the center of the EPR line and normalized to the half-power linewidth. The two solid lines correspond to 1D and 3D spin diffusion (see discussion in Sec. V).

The temperature dependence of the dc conductivity of POT-ES is well represented by $\sigma_{dc} \propto \exp[-(T_0/T)^{1/2}]$ with $T_0 = 30\,000$ K while the room-temperature value is ~ 0.01 S/cm (Fig. 7). Within the temperature range covered in the experiment (40–300 K) one can easily distinguish the applicability of the exponent $\frac{1}{2}$ from $\frac{1}{3}$ or $\frac{1}{4}$. For the sake of comparison, PAN-ES has the similar temperature dependence of σ_{dc} with $T_0 = 6000$ K and σ (295 K) $= 5 \times 10^{-1}$ S/cm. The microwave conductivity σ_{MW} of POT-ES at frequency 6.5 GHz has a similar value to

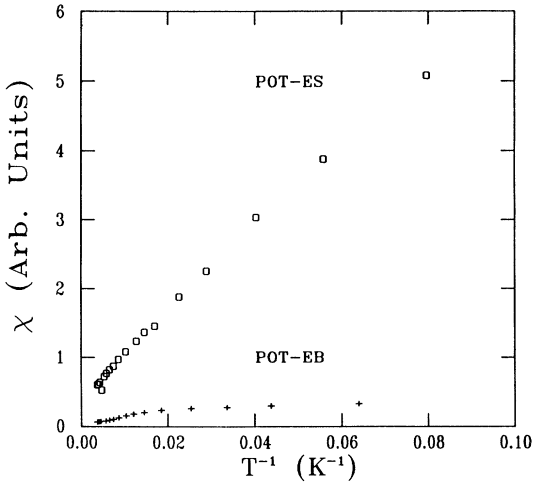

FIG. 3. Temperature dependence of EPR double integrals of POT-EB (+) and POT-ES (□) in arbitrary units. A finite χ at the $1/T \to 0$ limit in POT-ES suggests a finite χ_{Pauli}.

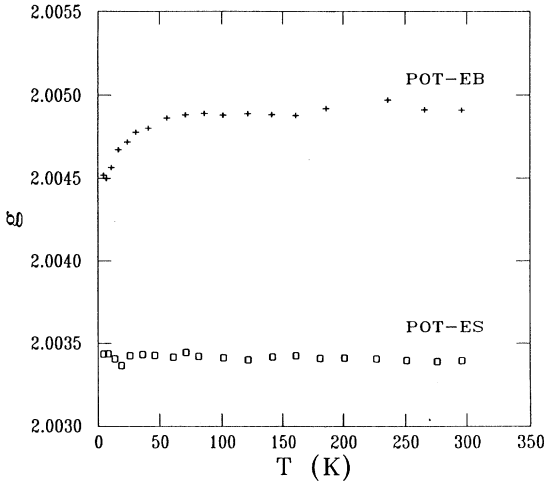

FIG. 5. Temperature dependence of EPR g factors of POT-EB (+) and POT-ES (□).

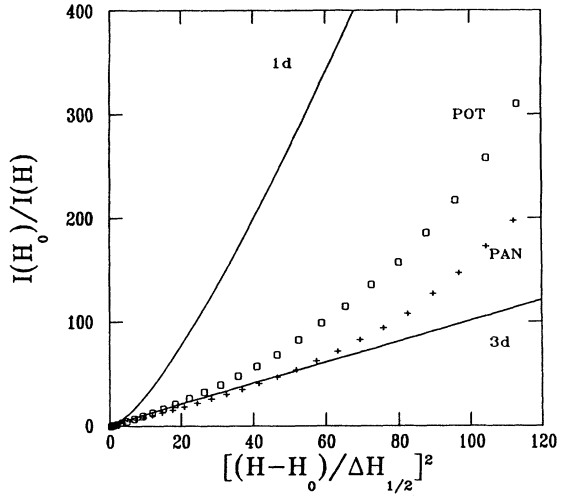

FIG. 6. The line-shape data of POT-ES (□) and PAN-ES (+) in comparison with the theoretical line shape of 1D and 3D spin diffusion. POT-ES is closer to 1D system behavior than PAN-ES.

that of σ_{dc} at room temperature, but is larger than σ_{dc} at low temperatures. The lower the temperature, the larger is the dispersion (Fig. 7). The microwave conductivity of that POT-EB is 5×10^{-4} S/cm at room temperature, while its dc conductivity is 10^{-10} S/cm. The microwave dielectric constant ϵ of POT-ES is about 10 at 295 K and 7 at 30 K, while ϵ of POT-EB is about 4.5 and independent of temperatures [inset (a) of Fig. 7].

It is noted that the room-temperature value of σ_{dc} may vary between 0.01 and 0.02 S/cm, depending on the sample conditions (moisture, doping level, sample age, etc.). For the extremely old samples (several months or a year in the atmosphere) σ_{dc} may be lowered to 3×10^{-3} S/cm. The old samples have much broader EPR linewidth (~2 G after several hours pumping) and large $S(T)$ (see below). The determination of the value of σ_{MW} requires the knowledge of the depolarization factor of the sample, which is difficult to calculate accurately due to the irregularity of the sample geometry. The value of the σ_{MW} in Fig. 7 was calculated from the measured sample dimensions. Changing the depolarization factor in a reasonably large range resulted in the change of σ_{MW} between 0.01 and 0.05 S/cm at 295 K.

The T dependence of thermoelectric power of POT-ES is approximately S_0+B/T with $S_0=-3.9$ μV/K and $B=1.6$ mV [inset (b) of Fig. 7]. At room temperature $S\sim2$ μV/K and increases when T is cooled down. For old samples, $S\sim10$ μV/K. Most of the samples show deviation from the S_0+B/T behavior in the vicinity of $T\sim300$ K with $S(T)$ slightly increasing with increasing temperature. It is also noted that $S(T)$ becomes slightly smaller (more negative) with exposure of samples to moisture (this may account for scatter in our data near room temperature).

The electric-field dependence of $\sigma(F)$ for POT-ES follows approximately the Poole-Frenkel formula[35]

$$\sigma(F)\propto\exp[\mathcal{K}(T)F^{1/2}]\ , \tag{18}$$

where the temperature-dependent constant $\mathcal{K}(T)$ decreases with the increase of the temperatures and electric field F is in the range of 1–400 V/cm (Fig. 8).

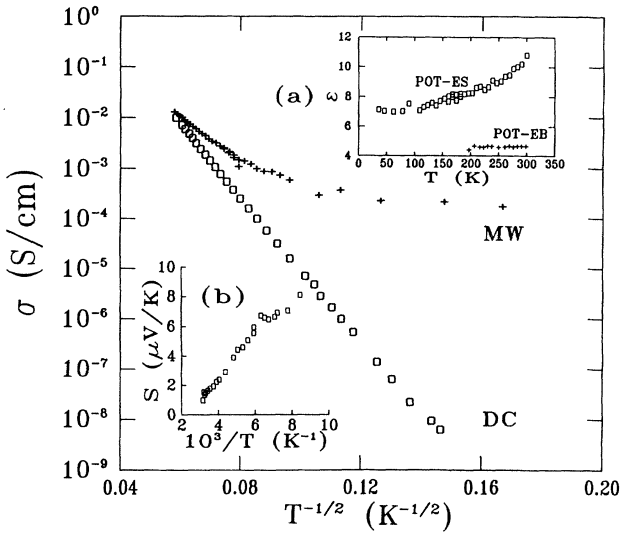

FIG. 7. T dependence of σ_{dc} (□) and σ_{MW} (6.5 GHz) (+) for POT-ES. Inset (a), T dependence of the dielectric constant of POT-ES (□) and POT-EB (+). There is a finite difference of ϵ in POT-ES and POT-EB. Inset (b), thermoelectric power $S(T)$ of POT-ES. Note that $S(T)=A+B/T$.

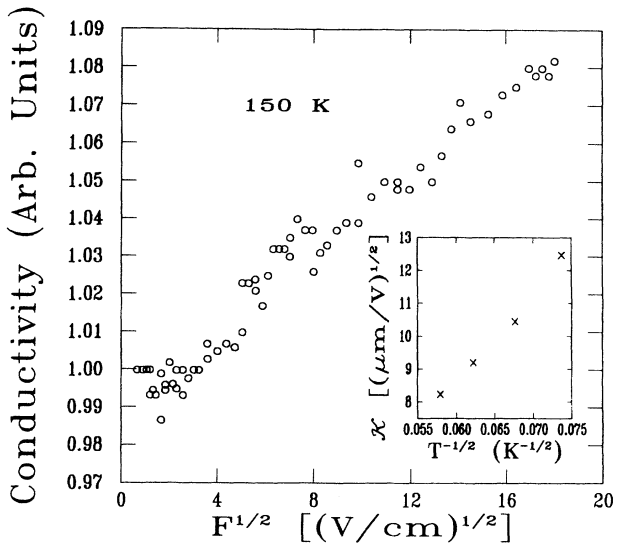

FIG. 8. The four-probe electric field (F) dependence of the conductivity $\sigma(F)$ at $T=150$ K vs $F^{1/2}$. The inset is the slope $\mathcal{K}(T)$ of the straight line in the figure at several different temperatures.

V. DISCUSSION

Upon HCl protonation the conductivity of POT increases from 10^{-10} to 10^{-2} S/cm. Earlier studies[15] showed that POT and PAN have similar optical spectra, suggesting similar band structures of the two polymers. However, our studies indicate that the conducting electrons in POT-ES are more localized compared with those in PAN-ES. The mechanism for this increased localization is investigated in this paper.

A. Magnetic properties

Static magnetic susceptibility of POT-ES may be decomposed into a finite Pauli-like component (temperture independent) and a Curie-like component ($\sim 1/T$), indicating the existence of a finite density state near the Fermi energy. From $\chi_{\text{Pauli}}=\mu_B^2 N(E_F)$, we calculate $N(E_F)=1.7$ states/eV per 2 rings. This suggest that conduction electrons in POT-ES are substantially delocalized and that their wave functions have extensive overlap with wave functions on neighboring sites. This decomposition is not good at low temperatures ($T<20$ K) where χ is smaller than expected (Fig. 2). This deviation may be due to a weak antiferromagnetic coupling from dipole-dipole interaction of adjacent spins or through bond coupling. This could also reflect a polaron to bipolaron transition at low temperatures.[33]

EPR linewidths of POT-ES and POT-ES are displayed in Fig. 4. Since both nitrogen and hydrogen have a nuclear magnetic moment, the hyperfine interaction between the electrons and the nuclei will broaden the EPR linewidth. A rough estimate of the hyperfine interaction between an electron and a proton gives

$$\Delta H=\frac{\mu_p}{r^3}\sim 10 \text{ G} , \tag{19}$$

where proton moment $\mu_p=1.4\times 10^{-23}$ erg/G and $r\sim 1$ Å. Although the EPR linewidth of POT-EB is on the order of 10 G in accordance with the above estimate, the EPR linewidth of POT-ES is at least one order smaller at room temperature. This difference is attributed to the electron motion which averages out the hyperfine interaction (and also other interactions like electron-electron dipole interactions) and narrows the EPR line (motional or exchange narrowing[36,37]). Therefore electron delocalization to some extent in POT-ES is expected in accord with the presence of a χ_{Pauli}. The decrease of EPR linewidth with increase of temperatures indicates that electron motion is increased as temperature increases.

Analysis of the EPR g factor of POT can result in a similar conclusion. The g factor of an electron near a carbon-hydrogen bond is about 2.0031, while it is 2.0054 for an electron near a nitrogen-hydrogen bond.[38] The g factor of POT-EB is close to 2.0054 (Fig. 5), indicating that radicals are localized to N sites only, but the g factor of POT-ES is $g=2.0034$ (Fig. 5), corresponding closely to the arithmetic mean of the g factors of six C and one N in the repeat unit, implying that electrons are delocalized over at least one ring and nitrogen repeat unit, i.e., ~ 5 Å. This gives a lower limit of the localization length of electrons in POT-ES.

A comparison of the magnetic properties of POT-ES with those of PAN-ES (Refs. 32, 33, and 39) is summarized in Table I. Though the total room temperature χ is the same, POT-ES has larger χ_{Curie} and smaller χ_{Pauli}. This implies greater electron localization in POT-ES.[40] Also POT-ES has a larger EPR linewidth than PAN-ES. This suggests there is less motional narrowing in POT-ES and hence electrons are more localized. In contrast, g factors of POT-ES and PAN-ES are similar, indicating the spins are delocalized over at least one ring and nitrogen repeat unit (~ 5 Å) for both polymers.

Note that $N(E_F)$ is closely related to bandwidth W. For a half-filled 1D band

$$N(E_F)=\frac{4}{\pi c W} , \tag{20}$$

where c is the lattice constant (2 ring-nitrogen units). Though $N(E_F)$ for POT-ES is approximately half of that for PAN-ES, it is not correct to conclude that POT-ES has twice as wide a bandwidth as PAN-ES. Instead, optical studies[15] suggest that POT-ES and PAN-ES have very similar bandwidths. Thus the apparent difference in $N(E_F)$ must come from the difference in either electron localization or electron-electron on-site interaction.[33] Note that since both polymers are inhomogeneous systems, χ_{Pauli} and χ_{Curie} may result from different regions (crystalline or amorphous) in the polymers.

Analysis of the EPR line shape shows that the spin diffusion in POT-ES is closer to 1D motion than that of PAN-ES. This is associated with the increased electron localization in POT-ES. For a system with 3D spin diffusion (diffusion rate $w >$ EPR linewidth $\Delta\nu$) the

TABLE I. Magnetic properties of POT-ES compared with PAN-ES (Ref. 33). N_{Curie} is the number of Curie spins per 2 rings and ΔH_{pp} is EPR peak-to-peak linewidth.

Quantities[a]	POT	ES
χ (10^{-6} emu/mol per 2 rings)	139	139
χ_{Pauli} (10^{-6} emu/mol per 2 rings)	54	110
N_{Curie} (per 2 rings)	0.065	0.023
EPR $\Delta H_{pp}(G)$	0.7	0.3
g factor	2.0034	2.0038

[a]All data are room-temperature values.

transverse magnetization $\Phi(t)$ varies such that $\Phi(t)\sim\exp(-t/t_0)$, resulting in a Lorentzian line shape;[41] for 1D spin diffusion (and also $w>\Delta\nu$), $\Phi(t)\sim\exp[-(t/t_0)^{-3/2}]$.[41,42] For a quasi-1D spin system with interchain spin diffusion, the EPR line shape is in between[41] and changes gradually from a 1D spin diffusion line shape to a 3D line shape while the interchain diffusion rate increases to become compatible with the intrachain diffusion rate or the EPR linewidth. The 1D and 3D theoretical line shapes as well as room-temperature experimental line shapes of POT-ES and PAN-ES are shown in Fig. 6. The POT-ES line shape is closer to 1D than that of PAN-ES.

It is noted that the analysis of the EPR line shape is not unique. The fitting of the POT-ES line shape at room temperature and low temperature (~4 K) to a simple 3D motional or exchange narrowing formula[36] gave reasonably good results. If this analysis were correct, our results would indicate that the spin-diffusion rate in POT-ES would be lower than that of PAN-ES, and not necessarily mean that POT-ES is closer to a 1D system than PAN-ES. However, a simple decomposition of the EPR line into a Lorentzian and a Gaussian component[32] was not successful. The analysis we adopt here (spin diffusion in 1D and 3D) is consistent with transport properties of POT-ES given in Sec. V B which show quasi-1D charge transport.

In summary, the electrons in POT-ES are greatly delocalized upon HCl doping from POT-EB, but they are still more localized than those in PAN-ES. This increased localization is associated with increased one-dimensionality of POT-ES compared with PAN-ES.

B. Transport properties

The increased electron localization in POT-ES can be also seen from T dependence of the dc conductivity. The room-temperature conductivity of POT-ES ($\sim10^{-2}$ S/cm) is two to three orders smaller than that of unoriented PAN-ES ($\sim5\times10^{-1}$–10^{1} S/cm). The temperature dependence of σ_{dc} of POT-ES (Refs. 18 and 44) is $\exp[-(T_0/T)^{1/2}$ (Fig. 7) with $T_0\sim30\,000$ K, much larger than $T_0=6000$ K obtained for PAN-ES.[43,44] Several models result in this kind of temperature dependence, including quasi-1D-VRH,[4,13,22] charging energy-limited tunneling for granular metal[19] and 3D-VRH with a Coulomb gap.[20] To probe the conduction mechanism thermoelectric power $S(T)$ and the electric-field dependence of the conductivity $\sigma(F)$ were measured. The $S(T)$ can be decomposed into the sum of a constant and $1/T$ term [inset (b) of Fig. 7], suggesting a quasi-1D VRH. Given a crystal structure with greater isolation between chains and the T dependence of $S(T)$, the σ_{dc} data are fit to the quasi-1D-VRH model Eq. (3) or Eq. (6), since interchain and intrachain resistance are in series and interchain σ ($\sigma_\perp$ or $\sigma_\parallel$) is much smaller than intrachain σ_{intra} for the case $w\ll w_c$. From the value of T_0 and $N(E_F)$ we estimate $\alpha^{-1}\sim0.88$ (2 rings) or roughly 9 Å, consistent with the above g-factor analysis.

We can also estimate the localization length from Eq. (14). The microwave dielectric constant of POT-ES and POT-EB has a finite difference about 2.5 at the $T=0$ limit. The dielectric constant of POT-EB is attributed to electronic polarization of the polymer backbone.[31] The difference $\epsilon=2.5$ is the contribution from the conduction electrons in POT-ES. From Eq. (15) and assuming $f=\frac{1}{3}$ for randomly oriented polymer chains, we estimate $l_i=1.2$ Å (Ref. 45) for $\epsilon=7.0-4.5=2.5$. Thus the localization length is $\alpha^{-1}=4l_i=5$ Å, in the same order as the estimated 9 Å obtained from T_0.

Note that l_i estimated from the data of both ϵ and T_0 is one order smaller than the crystalline coherent length (~40 Å).[16,17] There is also a significant amount of amorphous component in the polymer [~50% (Refs. 16 and 17)]. The measured l_i is an effective mean free path averaged over crystalline and amorphous regions. An alternative interpretation is that the measured ϵ is limited by the transverse polarization, rather than intrachain polarization. As interchain hopping dominates σ, the transvese polarization likely plays an important role in ϵ. The study of oriented polyaniline[46] favors this interpretation. Applying Eq. (16) to the transverse polarization, we get $\xi_\perp\sim5$ Å, on the order of the polymer chain dimension. This value suggests that electron wave functions are basically localized to one chain. In either limit (interchain or intrachain), ϵ implies the electron wave functions are localized to one chain and to regions less than crystalline coherence length.

The thermopower behavior of $S(T)=S_0+B/T$ is consistent with the quasi-1D-VRH model only. Though a similar behavior is also obtained in a semiconductor with an energy gap E_g at the Fermi energy[4] where $B=E_g/e$, from the data we obtain an unrealistic value for E_g of 1.6 meV, too small for the consistent application of the model (where $E_g\gg k_BT$ is required[4]). It is noted that phonon-drag effects cause the thermopower for pure crystalline metals and semiconductors to vary as $1/T$ at high temperature.[47] However, this effect can be observed only in highly crystalline samples[47] since disorder will suppress the phonon-drag effect.[48] Had it been observed, a phonon-drag peak would appear below 100 K and quickly disappear when T is raised. Phonon-drag effects at room temperature are negligible.[47]

As mentioned before, 3D VRH with a Coulomb gap also predicts[20] $\ln\sigma\sim-(T_0/T)^{1/2}$. However, analyses of dielectric, magnetic, and thermopower data argue against the applicability of this model. According to this model electron interactions cause the density of states $N(E)$ at the Fermi energy to vanish as $N(E)\propto(E-E_F)^2$. In a strong electron localization system where the transport properties are determined by single-particle hopping among the localized states, the dielectric constant provides a probe for $N(E_F)$ according to Eq. (16) (Refs. 27, 28, and 31)

$$\epsilon(T=0)\propto\alpha^{-2}N(E_F)\ . \tag{21}$$

However, the finite difference of ϵ for POT-ES and POT-EB at the $T=0$ limit [inset (a) of Fig. 7] indicates $\epsilon-\epsilon_\infty\propto N(E_F)\neq0$ where ϵ_∞ is taken as the dielectric constant of POT-EB. Finite χ_{Pauli} implies finite $N(E_F)$, which also contradicts the application of this model.

The thermopower for 3D VRH with a Coulomb gap is expected to be a constant[49] when $T \ll T_c$ where T_c is a critical temperature related to the Coulomb gap Δ. Here Δ (in eV) is determined by[49]

$$\Delta = \frac{e^2}{\epsilon^{3/2}} \frac{g(E_F)^{1/2}\pi^{3/4}}{\Gamma(5/2)^{1/2}} = 0.2 , \tag{22}$$

where $\Gamma(5/2)=1.329$. The critical temperature (T_c) (Ref. 49) (in K) is

$$T_c = 12\Delta^2/k_B^2 T_0 \sim 2000 . \tag{23}$$

For our experimental condition $T \ll T_c$, but $S(T)$ is *not* a constant. This is again inconsistent with the predictions of a Coulomb gap.

It is noted that the charging energy-limited tunneling model[19] (CELT) for granular metals also predicts $\ln\sigma \propto -T^{1/2}$. However, this theory predicts the electric-field dependence of conductivity $\sigma(F) \propto \exp(-F_0/F)$,[19] where F_0 is related to the size of the metallic grains.[19] This electric-field dependence is not consistent with the experimental results where $\sigma(F) \propto \exp(\mathcal{K}F^{1/2})$. The data of $\sigma(F)$ at higher field ($F \sim 10^4$ V/cm) and lower temperatures ($T=100$ K), utilizing two-probe techniques, were reported earlier.[50] Forcing a fit to the CELT model of the data at 10^4 V/cm results in the size d of the metallic regions being on the order of 1 μm.[50] This value is too large for the self-consistent application of the model, since the charging energy $E_c \sim e^2/\epsilon d \ll k_B T$ and hence is negligible.[50]

The dependence of σ on the electric field F can be modeled by Poole-Frenkel effects[35] where $\ln\sigma(F) \propto \mathcal{K}F^{1/2}$, as is shown in Fig. 8 where F is up to 400 V/cm. This field dependence is attributed to the change of an effective Coulomb potential $U(r)$ in the applied field F

$$U(r) = -\frac{e^2}{\epsilon r} - erF . \tag{24}$$

The potential is thus lowered by

$$\delta U = \left[\frac{4e^3}{\epsilon}\right]^{1/2} F^{1/2} . \tag{25}$$

In the case of quasi-1D-VRH, we consider that electrons are localized by effective Coulomb potentials between adjacent sites. The localization length α^{-1} is determined by[4]

$$\alpha^{-1} \approx \left[\frac{\hbar^2}{2mU}\right]^{1/2} , \tag{26}$$

which is changed by the electric field as well. Substituting Eq. (26) and Eq. (4) into Eq. (6) and expanding U in the first order of δU, we get

$$\ln\sigma = \frac{(T_0/T)^{1/2}}{4U}\left[\frac{4e^3}{\epsilon}\right]^{1/2} F^{1/2} + \text{const} = \mathcal{K}(T)F^{1/2} + \text{const} , \tag{27}$$

where

$$\mathcal{K}(T) = \frac{T_0^{1/2}}{2U}\left[\frac{e^3}{\epsilon}\right]^{1/2} T^{-1/2} = K' T^{-1/2} \tag{28}$$

and

$$K' = \frac{T_0^{1/2}}{2U}\left[\frac{2e^3}{\epsilon}\right]^{1/2} . \tag{29}$$

The experimental values of $\mathcal{K}(T)$ for different temperatures are shown in the inset of Fig. 8. Applying Eq. (28) for the linear relation between $\mathcal{K}(T)$ and $T^{-1/2}$ we obtained $K' \approx 0.24$ (cm K/V)$^{1/2}$. Using $T_0 = 30\,000$ K and $\epsilon \sim \epsilon_\infty = 4.5$ (choosing ϵ_∞ instead of ϵ is empirical[35]) for POT-ES, we find $U \approx 0.1$ eV. Utilizing Eq. (26) and $\alpha^{-1} \sim 9$ Å, we estimate the effective charge carrier mass $m \approx m_e$. This result suggests that the charge carriers for POT-ES are moving among the localized states without large C_6 ring motion characteristic of the massive polarons reported for the PAN-EB, leucoemeraldine base and lightly doped PAN-ES.[2,51]

Finally it is noted that the dispersion of σ is not significant between dc and 6.5 GHz at room temperature. This is not a surprising result if we calculate $\sigma_p(\omega)$ at $\omega = 2\pi \times 6.5$ GHz using Eq. (13) and $\nu_{ph} = 10^{13}$ Hz.[25] This yields $\sigma_p(\omega) \sim 10^{-3}$ S/cm at room temperature. This value is one order smaller than σ_{dc} at 300 K so that dispersion between dc and 6.5 GHz at room temperature is negligible, but at low temperatures the dispersion of the conductivity is large since σ_{dc} is decreased dramatically.

VI. LOCALIZATION MECHANISM

The magnetic and transport data show increasing localization in going from PAN-ES to POT-ES. There are several possible mechanisms for the increased electron localization in POT-ES compared with PAN-ES.

One is due to the reduced intrachain bandwidth of POT-ES. Since CH_3 is larger than H, the adjacent ring angles are increased to avoid the strong steric repulsion from CH_3 on the rings.[15] This reduces the overlap of the π-electron wave functions and hence the bandwidth.[2] Therefore electrons are more readily localized by a given magnitude of disorder.[4,52] Based on the optical studies[15] of POT-ES and PAN-ES, the variation in intrachain bandwidth between POT-ES and PAN-ES is less than 5%. Since $\alpha^{-1} \propto v_F^2 \propto W$,[5] there is only 5% reduction in α^{-1}, too small to account for the observed difference of the localization length in POT-ES and PAN-ES. Also other PAN derivatives, such as poly-*o*-ethoxyaniline, show almost identical intrachain bandwidth as PAN-ES, but their conductivities for unoriented samples are still two to three orders smaller than that of PAN-ES.[53]

Another fact is that CH_6 groups on the rings randomly locate on position (a) or (b) (see Fig. 1). This introduces an additional random potential along the chains which tends to reduce τ_i and thus decrease $w \propto \tau_i$. Since there is no significant broadening of the shoulders of the optical transition,[15] this random potential is expected to be

small. Chain defects or finite chain length of POT-ES may play some roles in localization. However, a molecular weight study[54] suggests that the chain length of POT ranges from 150 to 30 000 Å, much larger than localization length and even larger than crystalline coherence length ~40 Å.[16] Therefore the finite polymer chain length is unlikely to play an important role in the electron localization.

Finally we note that since POT-ES has a few percent increase in the interchain separations,[16] the interchain transfer will decrease. Also the interchain separation of POT-ES features more interchain disorder even within the crystalline regions.[16] Both effects will decrease the interchain diffusion rate and hence localize the electrons. We estimate the change in localization due to these two effects. We assume that due to the greater interchain disorder and the larger interchain separation in POT-ES there is no significant interchain coupling. Thus we can ignore the interchain diffusion in POT-ES. For PAN-ES, on the other hand, we assume that its chains pack into a perfect lattice within the crystalline regions and the interchain diffusion rate is characterized by a dimensionless parameter[11] $J=\pi t_\perp \tau_i/2^{1/2}\hbar$ where $\tau_i=l_i/v_F$. When $J=1$, a localization-delocalization transition occurs. Due to the interchain coupling, the localization length will be enhanced by a factor of ξ. If $J<1$, $\xi\approx 1/(1-J^2)$; if $J>1$, $\xi\approx N(1-1/J^2)$ (N is the number of the chains in a bundle determined by perpendicular coherence length of the crystalline regions). We take l_i to be the crystalline coherence length [40 Å (Ref. 17)], $v_F=2/\pi\hbar N(E_F)$ and $N(E_F)=3.5$/eV per 2 rings.[33] Assuming all the electron wave functions are exponentially decaying, we roughly estimate the transfer integral as[20]

$$t_\perp=\frac{2}{3}\frac{e^2}{\epsilon a}\frac{r}{a}\exp(-r/a)\ , \tag{30}$$

where r is the separation of two electron states, $\epsilon=4$,[31] and a is the radius of π electrons on the C atoms which is twice the value of the Bohr radius, i.e., 1.06 Å. Since the interchain separation of PAN-ES chains is about 5.5 Å, we assume $r=5.5$ Å.[16,17] This gives $t_\perp=0.066$ eV and $J\approx 3>1$. This analysis suggests that the crystalline regions of PAN-ES are in the metallic state with $\xi\sim N$.

Combining our transport and magnetic results with x-ray studies,[16] the mechanism for the increased localization in POT is proposed to be the reduced interchain diffusion rate due to the decreased interchain bandwidth $t_\perp$ caused by the larger tarnsverse unit cell length and more importantly the decreased coherence between the chains caused by greater disorder in interchain separation within the crystalline regions. Both of them are attributed to the existence of the CH_3 group on each C_6 ring. The CH_3 has larger size than H and its location on the (a) or (b) position of the C_6 ring varies depending on the ring rotation. Hence CH_3 increases the interchain spacing and induces more disorder in chain separation.

These results point to a methodology to synthesize materials of controlled one-dimensional character to further probe localization phenomena, through judicious increase or reduction in interchain coherence and separation. Similarly, the achievement of highly conducting "metallic" polymers then requires maximizing the interchain coherence and the interchain transfer integral. Increase of intrachain scattering time or conjugated length is also important and probably is easier to achieve by decreasing the defects, increasing the chain length, and stretching-orienting the polymer samples. Hence addition of the side groups to PAN and other polymers such as polypyrrole and polythiophene is likely to increase localization with concomitant decrease in conductivity in the absence of special crystal packing.[55]

VII. CONCLUSION

The electron localization phenomena in POT-ES were studied by the temperature dependence of the dc conductivity, electric-field dependence of the conductivity, microwave conductivity and dielectric constant, thermoelectric power, EPR and dc susceptibility measurements. The results showed greater electron localization in POT-ES compared with that of PAN-ES though their electronic band structures are very similar. X-ray studies of POT-ES and PAN-ES show similar crystallinity and intrachain coherence length of these two polymers. However, POT-ES has larger interchain separation and more disorder in the interchain separation. Combining these results with EPR line-shape analysis, it is proposed that the key factor for this localization is the decreased interchain diffusion rate caused by (1) reduced interchain bandwidth due to the larger size of the CH_3 group on each C_6 ring as compared with the H in PAN-ES which separates the neighboring chains further apart, and (2) reduced interchain coherence due to the enhanced disorder in interchain separation within the crystalline regions, likely induced by random location of CH_3 at (a) and (b) positions on C_6 ring. A rough estimate to account for the difference of interchain coupling in POT-ES and PAN-ES is consistent with this conclusion.

The slightly reduced intrachain bandwidth due to increased adjacent ring angles, small random potential along the chain introduced by the CH_3 on the ring, and finite chain length may play some roles, but they are not the primary causes of the difference of localization in POT-ES and PAN-ES. Their roles in electron localization of POT-ES are unlikely to be important.

The room-temperature conductivity of POT-ES is $\sim 10^{-2}$ S/cm, two to three orders smaller than that of PAN-ES ($\sim 5\times 10^{-1}$–10^{1} S/cm). The dielectric constant of POT-ES is also one order smaller (10 for POT-ES versus 100 for PAN-ES). POT-ES also has larger EPR line- width, more Curie spins, and fewer Pauli spins. The $\sigma_{dc}(T)$, $S(T)$, and $\sigma_{dc}(F)$ show that quasi-1D-VRH of the charge carriers between the nearest-neighboring chains is the conduction mechanism for POT-ES. This suggests that POT-ES is a quasi-1D-DS with weak interchain coupling. In the framework of the quasi-1D-VRH, electron localization length is found to be several angstroms, estimated from three independent experimental data: EPR g factor, T_0 from $\ln\sigma_{dc}(T)\propto -(T_0/T)^{1/2}$, and ϵ(6.5 GHz) at $T=0$ limit. If this model was also applied to the

electric-field dependence of $\sigma(F) \propto \exp(\mathcal{H}F^{1/2})$ and $\mathcal{H} \propto T^{-1/2}$, we conclude that the effective mass of the moving charges is on the order of the electron mass.

An important implication of our studies for polymer processing is discussed. Although increasing polymer chain length and reducing the defects on the polymer chain will increase the conductivity, the conductivity of the polymers is also limited by the interchain coherence and bandwidth. To improve the latter two parameters is very important.

ACKNOWLEDGMENTS

The authors thank Dr. H. H. S. Javadi and Dr. E. Ehrenfreund for experimental assistance and enlightening discussions, Mr. K. R. Cromack, J. Yue, and Dr. R. K. Kohli for assistance. This work is supported in part by the Defense Advanced Research Projects Agency through a contract monitored by U.S. Office of Naval Research and in part by National Science Foundation Materials Research Grant No. DMR-85-19059.

*Present address: Alchemi Research Center, Thanc-400601, Naharashtra, India.

[1]W. P. Su, J. R. Schrieffer, and A. J. Heeger, Phys. Rev. B **22**, 2099 (1980); M. J. Rice, Phys. Lett. **71A**, 152 (1979); S. A. Brazovskii, Zh. Eksp. Teor. Fiz. **78**, 677 (1980) [Sov. Phys.—JETP **51**, 342 (1980)].

[2]J. M. Ginder, A. J. Epstein, and A. G. MacDiarmid, Solid State Commun. **72**, 697 (1989); J. M. Ginder and A. J. Epstein, Phys. Rev. B **41**, 10674 (1990).

[3]N. F. Mott and W. D. Twose, Adv. Phys. **10**, 107 (1961); N. F. Mott, Adv. Phys. **16**, 49 (1967); R. E. Borland, Proc. R. Soc. London, Ser. A **274**, 529 (1963); R. E. Borland and N. E. Bird, Proc. Phys. Soc. London **83**, 23 (1964).

[4]N. F. Mott and E. Davis *Electron Processes in Non-crystalline Matter* (Clarendon, Oxford, 1979).

[5]A. A. Gogolin, Phys. Rep. **1**, 1 (1982); **5**, 269 (1988).

[6]Y. A. Firsov, in *Localization and Metal Insulator Transition,* edited by H. Fritzsche and D. Adler (Plenum, New York, 1985), p. 477.

[7]S. Kivelson and A. J. Heeger, Synth. Met. **22**, 371 (1988).

[8]H. Naarmann and N. Theophilou, Synth. Met. **22**, 1 (1987); J. Tsukamoto, A. Takahashi, and K. Kawasaki, Jpn. J. Appl. Phys. **29**, 125 (1990); H. H. S. Javadi, A. Chakraborty, C. Li, N. Theophilou, D. B. Swanson, A. G. MacDiarmid, and A. J. Epstein, Phys. Rev. B **43**, 218 (1991); N. Theophilou, D. B. Swanson, A. G. MacDiarmid, A. Chakraborty, H. H. S. Javadi, R. P. McCall, S. P. Treat, F. Zuo, and A. J. Epstein, Synth. Met. **28**, D35 (1989); T. Schimmel, W. Reiss, J. Gimeiner, G. Denninger, M. Schwoerer, H. Naarmann, and N. Theophilou, Solid State Commun. **65**, 1311 (1988); A. J. Epstein, H. Rommelman, R. Bigelow, H. W. Gibson, D. M. Hoffman, and D. B. Tanner, Phys. Rev. Lett. **50**, 1866 (1983).

[9]See, for example, *Handbook of Conducting Polymers,* edited by T. A. Skotheim (Dekker, New York, 1986), Vol. 2.

[10]L. Pietronero, Synth. Met. **8**, 225 (1983).

[11]V. N. Prigodin, Y. A. Firsov, and W. Weller, Solid State Commun. **59**, 729 (1986).

[12]P. A. Lee and T. V. Ramakrishnan, Rev. Mod. Phys. **57**, 287 (1985).

[13]E. P. Nakhmedov, V. N. Prigodin, and A. N. Samukhin, Fiz. Tverd. Tela (Leningrad) **31**, 31 (1989) [Sov. Phys.—Solid State **31**, 368 (1989)].

[14]R. H. Baughman and L. W. Shacklette, Phys. Rev. B **39**, 5872 (1989); L. W. Shacklette and R. H. Baughman, Mol. Cryst. Liq. Cryst. **189**, 193 (1990).

[15]Y. Wei, W. W. Focke, G. E. Wnek, A. Ray, and A. Ray, A. G. MacDiarmid, J. Phys. Chem. **93**, 495 (1989); A. Ray, A. G. MacDiarmid, J. M. Ginder, and A. J. Epstein, Proc. Mater. Res. Soc. **173**, 353 (1990); Z. H. Wang, A. J. Esptein, A. Ray, and A. G. MacDiarmid, Synth. Met. (to be published).

[16]M. E. Józefowicz, A. J. Epstein, J. P. Pouget, J. G. Masters, A. Ray, Y. Sun, X. Tang, and A. G. MacDiarmid, Synth. Met. (to be published).

[17]M. E. Józefowicz, R. Laversanne, H. H. S. Javadi, A. J. Epstein, J. P. Pouget, X. Tang, and A. G. MacDiarmid, Phys. Rev. B **39**, 12958 (1989); J. P. Pouget, M. E. Józefowicz, A. J. Esptein, X. Tang, and A. G. MacDiarmid, Macromolecules **24** (1991).

[18]Z. H. Wang, H. H. S. Javadi, A. Ray, A. G. MacDiarmid, and A. J. Epstein, Phys. Rev. B **42**, 5411 (1990).

[19]P. Sheng and B. Abeles, Phys. Rev. Lett. **28**, 34 (1972).

[20]B. I.Shklovskii and A. L. Efros, *Electronic Properties of Doped Semiconductors* (Springer-Verlag, New York, 1984).

[21]J. Kurkijarvi, Phys. Rev. B **8**, 922 (1973).

[22]V. K. S. Shante, C. M. Varma, A. N. Bloch, Phys. Rev. B **8**, 4885 (1973).

[23]A. Miller and E. Abrahams, Phys. Rev. **120**, 745 (1960).

[24]D. Emin, Phys. Rev. Lett. **32**, 303 (1974).

[25]P. Nagels, in *Amorphous Semiconductors,* edited by M. H. Brodsky (Springer-Verlag, New York, 1979), p. 114.

[26]A. R. Long, Adv. Phys. **31**, 553 (1982).

[27]R. L. Bush, Phys. Rev. B **13**, 805 (1976).

[28]N. F. Mott, Adv. Phys. **34**, 329 (1985).

[29]P. M. Chaikin and J. F. Kwak, Rev. Sci. Instrum. **46**, 218 (1975).

[30]L. Buravov and I. F. Shchegolev, Prib. Tekh. Eksp. **2**, 171 (1971) [Instrum. Exp. Tech. (USSR) **14**, 528 (1971)].

[31]H. H. S. Javadi, K. R. Cromack, A. G. MacDiarmid, and A. J. Epstein, Phys. Rev. B **39**, 3579 (1989).

[32]H. H. S. Javadi, R. Laversanne, A. J. Esptein, R. K. Kohli, E. M. Scherr, and A. G. MacDiarmid, Synth. Met. **29**, E439 (1989).

[33]J. M. Ginder, A. F. Richter, A. G. MacDiarmid, and A. J. Epstein, Solid State Commun. **63**, 97 (1987).

[34]L. N. Mulay and E. A. Boudreaux, *Theory and Applications of Molecular Diamagnetism* (Wiley, New York, 1976).

[35]N. F. Mott, Philos. Mag. **24**, 911 (1971).

[36]R. Kubo and K. Tomita, J. Phys. Soc. Jpn. **9**, 888 (1954).

[37]N. M. Atherton, *Electron Spin Resonance* (Wiley, New York, 1973).

[38]J. R. Morton, Chem. Rev. **64**, 453 (1964).

[39]P. Vaca, M. E. Józefowicz, A. J. Epstein, X. Tang, and A. G. MacDiarmid (unpublished); R. Laversanne, H. H. S. Javadi, P. Vaca, A. J. Epstein, R. K. Kohli, E. Scherr, and A. G. MacDiarmid (unpublished).

[40]M. Milovanovic, S. Sachdev, and R. N. Bhatt, Phys. Rev. Lett. **63**, 82 (1989).

[41]M. J. Hennessy, C. D. McElwee, and P. M. Richards, Phys. Rev. B **7**, 930 (1973).

[42]R. E. Dietz, F. R. Merritt, R. Dingle, D. Hone, G. Sibernagel,

and P. M. Richards, Phys. Rev. Lett. **26**, 1186 (1971).
[43]F. Zuo, M. Angelopoulos, A. G. MacDiarmid, and A. J. Epstein, Phys. Rev. B **36**, 3475 (1987).
[44]There is no difference in σ_{dc} data for PAN-ES samples obtained on films (Ref. 43) and pressed powders.
[45]This can be compared to $l_i = 3.8$ Å estimated for 50% protonated PAN-ES. Noting $l_i = 0.7$ Å by Javadi *et al.* (Ref. 31) for PAN-ES should be 2.7 Å with 4π correction of Eq. (2) in Ref. 31.
[46]Z. H. Wang, C. Li, E. Scherr, A. G. MacDiarmid, and A. J. Epstein (unpublished).
[47]D. K. C. MacDonald, *Thermoelectricity: An Introduction To The Principles* (Wiley, New York, 1962); Jan Taug, *Photo and Thermoelectric Effects In Semiconductors* (Pergamon, Oxford, 1962).
[48]J. Jackle, J. Phys. F **10**, L43 (1980).
[49]M. J. Burns and P. M. Chaikin, J. Phys. C **18**, L743 (1985).
[50]Z. H. Wang, E. Ehrenfreund, A. Ray, and A. G. MacDiarmid, Liq. Cryst. Mol. Cryst. **189**, 263 (1990).
[51]R. P. McCall, J. M. Ginder, M. G. Roe, G. E. Asturias, E. M. Scherr, A. G. MacDiarmid, and A. J. Epstein, Phys. Rev. B **39**, 10174 (1989); R. P. McCall, J. M. Ginder, J. M. Leng, H. J. Ye, S. K. Manohar, J. G. Master, G. E. Asturias, A. G. MacDiarmid, and A. J. Epstein, *ibid.* **41**, 5202 (1990).
[52]P. W. Anderson, Phys. Rev. **109**, 1492 (1958); Rev. Mod. Phys. **50**, 470 (1978).
[53]S. K. Manohar, A. G. MacDiarmid, and A. J. Epstein, Bull. Am. Phys. Soc. **34**, 583 (1989); (unpublished).
[54]Y. Wei, K. F. Hsueh, S. Nagy, A. Ray, A. G. MacDiarmid, J. Dykins, A. J. Epstein, and G. E. Wnek, Proc. Res. Soc. **173**, 341 (1990).
[55]V. Enkelmann, J. Rühe, and G. Wagner, Synth. Met. **37**, 79 (1990).